



Cite this: *RSC Adv.*, 2022, 12, 28349

A colorimetric sensing platform for the determination of H_2O_2 using 2D–1D MoS_2 -CNT nanozymes †

Xin Zhang, Siqin Wang, Jiahao Dao, Jiajing Guo and Yanfang Gao *

A novel colorimetric platform based on nano-composites of two-dimensional (2D) molybdenum disulfide nanosheets (MoS_2 NSs) and one-dimensional (1D) carbon nanotubes (CNTs), called 2D–1D MoS_2 -CNT nanozyme, was fabricated for the selective and sensitive determination of hydrogen peroxide (H_2O_2) in soda water. The MoS_2 -CNT nanozyme was synthesized through a one-step solvothermal reduction method. The introduced CNTs could effectively prevent the stacking of MoS_2 nanosheets (NSs) and not only expanded the interlayer distance of MoS_2 NSs from 0.620 nm to 0.710 nm but also improved their specific surface. Under acidic conditions, the as-prepared 2D–1D MoS_2 -CNT nanozymes could oxidize the colorless 3,3',5,5'-tetramethylbenzidine (TMB) to blue-oxidized TMB (oxTMB) in the presence of H_2O_2 , resulting in enhanced peroxidase-like (POD-like) activity. The kinetic study showed that MoS_2 -CNT nanozyme had stronger catalytic activity than natural horseradish peroxidase (HRP). The linear range for H_2O_2 colorimetric determination was 5.00–500 $\mu\text{mol L}^{-1}$ with a limit of detection (LOD) of 1.40 $\mu\text{mol L}^{-1}$. Furthermore, the established determination method was applied to actual samples and the recoveries of H_2O_2 spiked in soda water were in the range of 92.3–107%, showing feasibility for the analysis of food.

Received 3rd August 2022
Accepted 15th September 2022

DOI: 10.1039/d2ra04831k

rsc.li/rsc-advances

Introduction

Nanozymes are new artificial enzymes, which have the characteristics of both nanomaterials and natural enzymes.^{1,2} However, compared with traditional natural enzymes, nanozymes have a series of unique advantages such as high stability, low cost and easy preservation.^{3,4} Therefore, increasing research is devoted to related fields, including biomedical diagnostics,^{5,6} food safety,⁷ environmental monitoring⁸ and antibacterial agents.⁹ Given that H_2O_2 plays an important role in the above-mentioned fields, its determination is of great interest.^{10,11} The determination of H_2O_2 is usually achieved using nanomaterials with POD-like activity, which catalyze the H_2O_2 -mediated oxidation of typical substrates.⁴

MoS_2 NSs possess a graphite-like layered structure, which is stacked by S–Mo–S through van der Waals forces. Many studies have revealed that MoS_2 NSs can oxidize colorless TMB to blue oxTMB in the presence of H_2O_2 under acidic conditions. Thus, MoS_2 NSs are considered to have POD-like activity.¹² However, the stacking of the MoS_2 NS layers severely limits the exposure of their catalytic active sites. At present, some methods have been used to expand the interlayer distance between MoS_2 NSs

and improve their POD-like performance. In our previous work, the interlayer distance of MoS_2 NSs was expanded from 0.620 to 0.810 nm by doping Ce^{3+} in MoS_2 .¹³ In another work, 2D hexagonal boron nitride (h-BN) was combined with MoS_2 NSs to form a 2D/2D h-BN/ MoS_2 NS heterogeneous catalyst, and the interlayer distance of the MoS_2 NSs increased from 0.620 to 0.700 nm.¹⁴ In conclusion, the above-mentioned two methods can broaden the spacing of MoS_2 NSs, improve their contact with H_2O_2 , and improve their ability for the catalytic decomposition of H_2O_2 .

CNTs have a series of advantages such as high surface area, excellent electronic conductivity and optical properties, and thus widely applied in various fields.^{15–17} It has been proved that CNTs can promote the electron transfer ability and effectively avoid the accumulation of MoS_2 NSs.¹⁸ Nanocomposites of MoS_2 and CNTs have been investigated widely for energy storage and catalytic applications. Zhang *et al.*¹⁷ prepared MoS_2 /CNT core-shell nanocomposites with enhanced the nonlinear optical (NLO) performances. Miao's group¹⁹ synthesized homogeneous CNT- MoS_2 -carbon *via* the wet impregnation method and calcination and employed it as counter electrodes (CEs) in dye-sensitized solar cells (DSSCs). The CEs exhibited a low charge transfer resistance and excellent photoelectric conversion efficiency. Han *et al.*²⁰ used a CNT-modified exfoliation method to obtain few-layer MoS_2 NSs, which exhibited an excellent electrochemical performance for both sodium-ion storage and hydrogen evolution. However, the catalytic H_2O_2 mechanism of

College of Chemical Engineering, Inner Mongolia University of Technology, 49 Aimin Road, Hohhot, 100085, China. E-mail: yf_gao@imut.edu.cn

† Electronic supplementary information (ESI) available. See <https://doi.org/10.1039/d2ra04831k>



single-wall carbon nanotubes (SWNTs) is still controversial.^{21,22} Some researchers believe that it is related to the trace metal catalyst in SWNTs. It was only in 2010 that Qu and co-workers²³ confirmed for the first time that SWNTs possess intrinsic POD-like activity.

Herein, we prepared 2D–1D MoS₂-CNT nanozyme *via* a simple one-step hydrothermal reduction method. In the growth process of MoS₂ NSs, the introduction of CNTs prevented the stacking of the MoS₂ NSs and increased their inter-layer distance and specific surface area. Owing to the synergistic effect of the MoS₂ NSs and CNTs, the MoS₂-CNT nanozymes exhibited enhanced ability for the catalytic decomposition of H₂O₂. Consequently, based on this, a sensitive and reliable MoS₂-CNT/TMB/H₂O₂ platform was constructed. The colorimetric detection platform exhibited a wide linear range and low limit of detection (LOD).

Experimental

Materials and reagents

Ammonium thiomolybdate ((NH₄)₂MoS₄), TMB, dopamine hydrochloride (DA, 98%) and *N,N*,dimethylformamide (DMF) were purchased from Aladdin Reagent Co., Ltd. L-Lysine (L-Lys) and L-arginine (L-Arg) were purchased from Sangon Biotech Co., Ltd. 30.0% H₂O₂, sodium acetate (NaAc, 99.0%), D(+)-glucose, acetic acid (HAc, 99.5%), hydrazine hydrate (N₂H₄·H₂O), sodium chloride (NaCl, 99.5%), and ammonia chloride (NH₄Cl, 99.5%) were obtained from Sinopharm Chemical Reagent Co., Ltd. Carbon nanotubes were purchased from Chinese Academy of Sciences Chengdu Organic Chemistry Co., Ltd. All reagents were of analytical grade unless otherwise stated.

Instrumentation

The morphology and structure of the MoS₂-CNT nanozyme was characterized *via* emission scanning electron microscopy (SEM, Hitachi-SU8220) and transmission electron microscopy (TEM, JEM-2010). X-Ray diffraction (XRD) patterns were recorded on a Rigaku Smartlab 9 KW with Cu K α radiation. The 2 θ values were recorded at a step size of 0.02° in the scan range of 5.00–70.0°. Raman spectroscopy was performed on a Renishaw *in via* Reflex Laser Micro-Raman spectrometer at an excitation wavelength of 532 nm. Thermogravimetric analysis (TGA) was carried out using an STA449 F3 Jupiter instrument under air flow at a heating rate of 10 °C min^{−1} from 30 °C to 1300 °C. X-ray photoelectron spectroscopy (XPS) was performed using a Thermo-Fisher ESCALAB 250Xi system with an Al K α source. Nitrogen adsorption-desorption isothermal curves were measured at 77 K using a BeiShide 3H-2000PS2. The specific surface area and pore size distribution were obtained by Brunauer-Emmett-Teller (BET) and Barrett-Joyner-Halenda (BJH) analyses. UV-vis spectra were recorded using a Shimadzu UV-2550 spectrophotometer.

Synthesis of the MoS₂-CNT nanozyme

According to the literature,²⁴ the MoS₂-CNT nanozyme was prepared *via* one-step solvothermal reduction. Firstly, 66.0 mg

(NH₄)₂MoS₄ was dissolved in 15 mL DMF solution, and 30.0 mg CNTs was evenly dispersed in 15.0 mL DMF solution. Then, the aforementioned two solutions were mixed and sonicated until a uniform solution was formed. Subsequently, 300 μ L N₂H₄·H₂O was added dropwise to the above-mentioned solution and continuously stirred for 30 min. Then, the mixed solution was transferred to a 50.0 mL teflon-lined stainless steel autoclave and reacted at 200 °C for 10 h. The autoclave was allowed to cool naturally. The black powder was collected by centrifugation and washed three times with ultrapure water and anhydrous ethanol alternately. The final products were dried at 80.0 °C for 12 h. The prepared material was named as MoS₂-CNT nanozyme. For comparison, the method for the synthesis of the MoS₂ nanozyme was the same as that for the MoS₂-CNT nanozyme but without the CNTs.

POD-like activity assay

The POD-like activity of the MoS₂-CNT nanozyme was evaluated by the oxidation of the colourless TMB to blue oxTMB in the presence of H₂O₂. The total volume of the reaction was 4.00 mL, including 40.0 μ L 1.00 mg mL^{−1} MoS₂-CNT nanozymes, 20.0 μ L 30.0% H₂O₂ solution, 40.0 μ L 10.0 mmol L^{−1} TMB and 3.90 mL 100 mmol L^{−1} acetic acid-sodium acetate (HAc-NaAc) buffer (pH = 4.00). The solution was thoroughly mixed and placed in a 10.0 °C water bath for 40 min. The absorbance value at the wavelength of 652 nm was recorded using a UV-vis spectrometer.

Optimization of POD-like catalytic conditions

The effects of reaction time, temperature, pH and substrate concentration on the reaction system were investigated, respectively, where only one of these conditions was changed in each test. The absorbance was measured at 652 nm wavelength. At least three parallel samples were measured for each experiment.

Apparent kinetic assay

The POD-like catalytic mechanism of the MoS₂-CNT nanozyme was investigated *via* a steady-state kinetic assay. TMB and H₂O₂ were selected as the substrates. The tests were carried out by varying the concentration of TMB at a fixed H₂O₂ concentration under the optimal conditions described above, and *vice versa*. Each experiment was repeated three times. The kinetics constants were determined by double reciprocal plots and eqn (1), where K_m is the Michaelis constant, V_0 is the initial reaction rate, V_{max} is the maximum reaction rate, and $[S]$ is the substrate concentration.

$$\frac{1}{V_0} = \frac{K_m}{V_{max}} \cdot \frac{1}{[S]} + \frac{1}{V_{max}} \quad (1)$$

Colorimetric determination of H₂O₂

The colorimetric determination of H₂O₂ was carried out using the following system: 40.0 μ L of 1.00 mg mL^{−1} MoS₂-CNTs, 320 μ L of 800 μ mol L^{−1} TMB, and 20.0 μ L of H₂O₂ with different



concentrations. The reaction system was supplemented with 4.00 mL of 100 mmol L⁻¹ HAc-NaAc buffer (pH = 4.00). The absorbance at 652 nm was measured under the optimal conditions, and the calibration curve of H₂O₂ concentration *vs.* absorbance was plotted. Next, the LOD of the reaction system was calculated using the formula $LOD = 3S/k$, where “S” is the relative standard deviation of 11 controls without H₂O₂ and “k” is the slope of the linear curve.

Selective experiment

Glucose, dopamine (DA), lysine (Lys), arginine (Arg), ammonium ion (NH₄⁺) and sodium ion (Na⁺) were used as interferents to investigate the selectivity of the reaction system. In this experiment, the concentrations of these interferents were adjusted to 5-times the concentration of H₂O₂ and replaced H₂O₂. Under the optimum reaction conditions, the UV-vis absorbance of the reaction system in the presence of interferents was recorded at a wavelength of 652 nm. All data were measured three times under the same conditions, and the average value was employed to draw the curve.

Results and discussion

Characterization of MoS₂-CNT nanozyme

The morphology of MoS₂, CNTs and MoS₂-CNT nanozyme was investigated using SEM and TEM. Fig. S1(a and b†) show the typical SEM and TEM images of MoS₂, respectively, which presents a layered and stacked structure. Fig. S1(c and d†) reveal the SEM and TEM images of the CNTs, respectively, which show a tubular structure with a length of several microns. Fig. 1a and b reveal the typical SEM images of the MoS₂-CNT nanozyme, consisting of layered MoS₂ NSs interleaved with tubular CNTs. The TEM image of the MoS₂-CNT nanozyme (Fig. 1c) further exhibits the typical crinkly structure of MoS₂ connected with

CNTs. The HRTEM image (Fig. 1d) indicates that the interplanar spacing of the CNTs is 0.320 nm, which corresponds to the (002) crystal plane of the CNTs.²⁵ The other interlayer spacing of about 0.700 nm corresponds to the (002) crystal plane of MoS₂. Obviously, it is larger than that of the pristine MoS₂ (0.620 nm), which indicates that the introduction of CNTs inhibited the stacking of the MoS₂ NSs and expanded their interlayer distance.

The structural characteristics of the as-prepared MoS₂-CNT nanozyme were characterized by XRD and the results are shown in Fig. 2a. In the XRD pattern of MoS₂, the diffraction peaks located at 9.18° and 17.3° correspond to the (001) and (002) crystal planes of 2H-MoS₂ (JCPDS No.73-1508), while the other two peaks at 33.1° and 57.9° in the high-angle region correspond to the (100) and (110) planes of 2H-MoS₂, respectively. The other diffraction peak at 26.1° belongs to the (002) plane of CNTs.²⁶ The as-prepared nanozymes possessed both the (001) diffraction peak of MoS₂ and (002) diffraction peak of CNTs. Compared with the original MoS₂, the (001) of the MoS₂-CNT nanozyme shifted towards the low-angle region, and the half-peak width increased, accompanied by a decrease in peak intensity. This shows that the introduction of CNTs expanded the inter-layer distance of MoS₂, which is consistent with the HRTEM results. Fig. 2b reveals the Raman spectra of MoS₂, CNTs and MoS₂-CNT nanozyme in a wide spectral range. The two characteristic bands at 375 and 400 cm⁻¹ correspond to the in-plane E_{2g} and out-of-plane A_{1g} modes of hexagonal MoS₂, respectively.²⁷ Moreover, the other two peaks at about 1345 cm⁻¹ and 1585 cm⁻¹ belong to the D band and G band of the pristine CNTs, respectively. The D band corresponds to sp²-hybridized carbon, while the G band originates from sp³-hybridized carbons.²⁸ Usually, the D band is associated with the structural defects or disorders present in CNTs, whereas the G band reflects the properties of all carbon materials. In contrast,

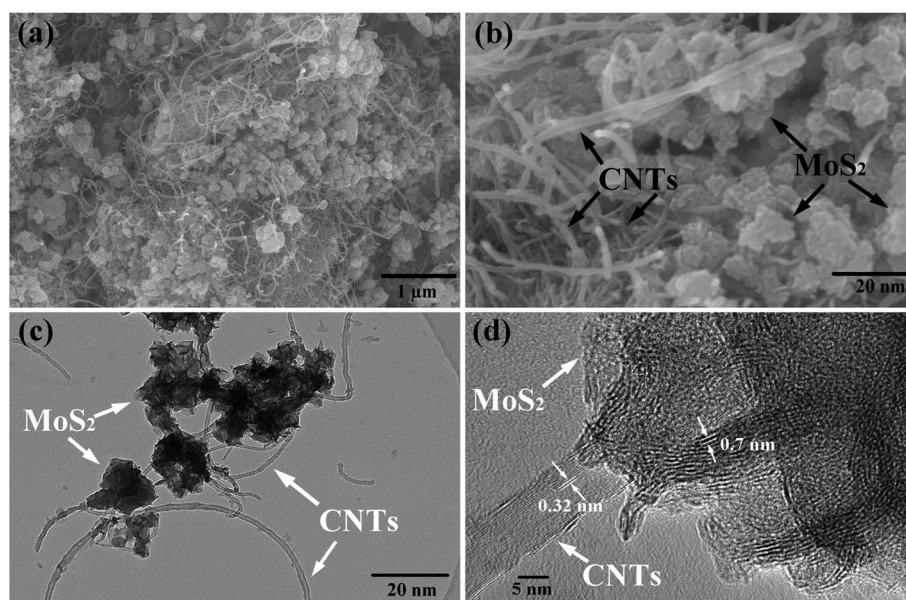


Fig. 1 (a) and (b) SEM, (c) TEM, and (d) HRTEM images of MoS₂-CNT nanozyme.

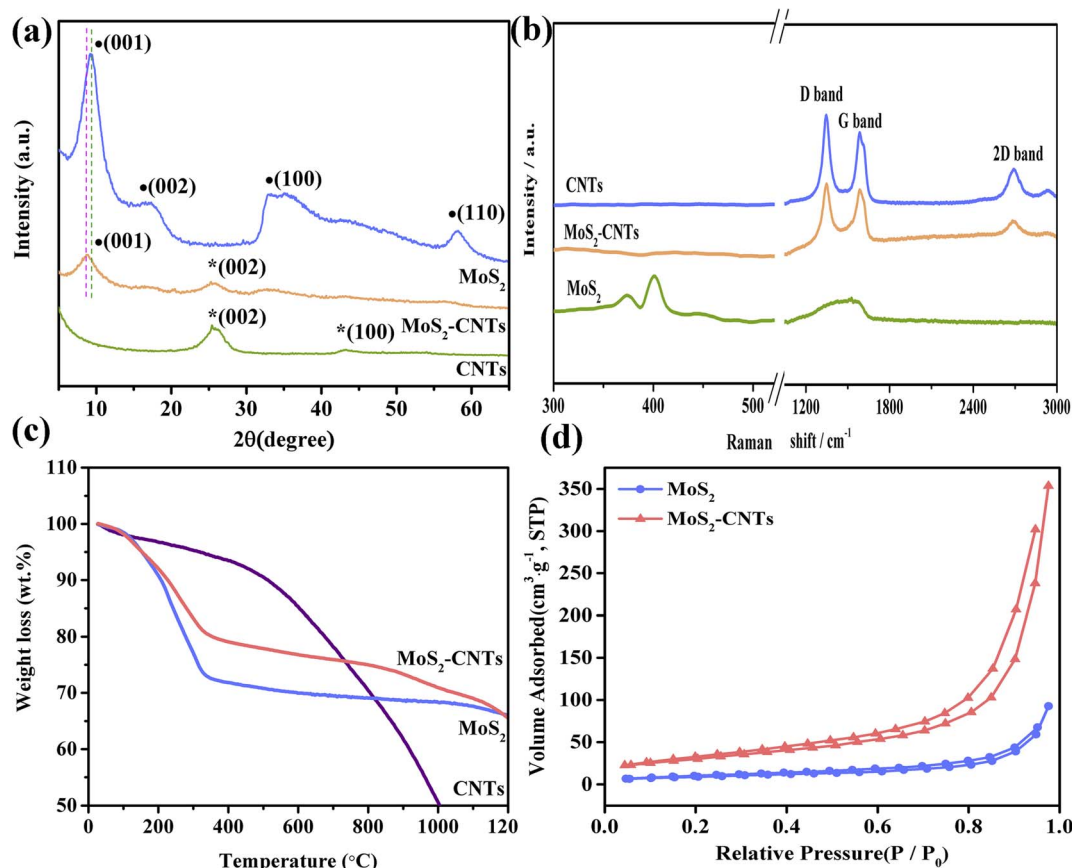


Fig. 2 (a) XRD patterns, (b) Raman spectra, (c) TGA curves, and (d) N₂ adsorption-desorption curves of CNTs, MoS₂ and MoS₂-CNT nanozyme.

in the MoS₂-CNT nanozyme, the peak positions of both the D and G bands were slightly red shifted. This shift may be related to the strong interfacial interaction between the CNTs and MoS₂.¹⁷ In addition, the 2D peak at 2691 cm⁻¹ is a second-order D band, which is caused by the double vibrational Raman scattering.²⁷

Furthermore, the thermal stability of the as-prepared MoS₂-CNT nanozymes was obtained by TGA. As shown in Fig. 2c, for the CNTs, the first significant weight loss occurred approximately between 30–500 °C due to the presence of some amorphous carbon in the CNT matrix. Then the CNTs themselves burned in the temperature range of 500–1000 °C.²⁹ Up to 1000 °C, the sample still retained about 50% of its weight, showing extremely high thermal stability. MoS₂ and MoS₂-CNT nanozymes displayed a similar weight loss tendency in the range of 30–1200 °C. In the case of the MoS₂-CNT nanozymes, the weight loss process was roughly divided into four stages. The first weight loss of about 2% is due to the evaporation of water in the range of 30–150 °C. The second weight loss stage occurred in the range of 150–350 °C, with approximately 20% weight loss, which was caused by the oxidation of MoS₂ in the air atmosphere. The third stage (about 5%) was caused by the oxidation of the CNTs in the range of 350–900 °C. In the last stage, the weight of the MoS₂-CNT nanozymes decreased by only about 8%, indicating that it has favourable high thermal

stability. Obviously, the weight loss of the MoS₂-CNT nanozymes was less than that of the pure MoS₂, which proves that the introduction of CNTs improved the thermal stability of MoS₂. Fig. 2d exhibits the N₂ adsorption-desorption isotherms of MoS₂ and MoS₂-CNT nanozymes. The isotherms show the typical type-IV curves with H₃-type hysteresis loops. The MoS₂-CNT nanozymes (110 m²g⁻¹) had an increased specific surface area compared with the pure MoS₂ NSs (32.8 m²g⁻¹).

To further investigate the components of the as-prepared MoS₂-CNT nanozyme, XPS was performed. Fig. 3a shows the XPS survey spectrum of the MoS₂-CNT nanozyme, indicating the presence of C, Mo, S, O and N elements. The high-resolution C 1s spectrum (Fig. 3b) can be divided into three peaks with binding energies at 284.7, 285.8 and 289.0 eV, which correspond to the sp² C=C, sp³ C-C and C-O bonds of the CNTs, respectively. In the high-resolution spectrum of Mo 3d (Fig. 3c), the two pairs of significant peaks located at 228.8/229.9 eV and 232.1/233.1 eV correspond to Mo 3d_{5/2} and Mo 3d_{3/2}, respectively. The peak at 235.8 eV is ascribed to Mo⁶⁺, indicating the partial oxidation of the material surface. The other peak at 226.2 eV is ascribed to S 2s, indicating the presence of sulfur in the compounds.^{30,31} In the S 2p spectrum (Fig. 3d), the peaks at 161.7 and 163.0 eV are ascribed to S 2p_{3/2} and S 2p_{1/2}, respectively.



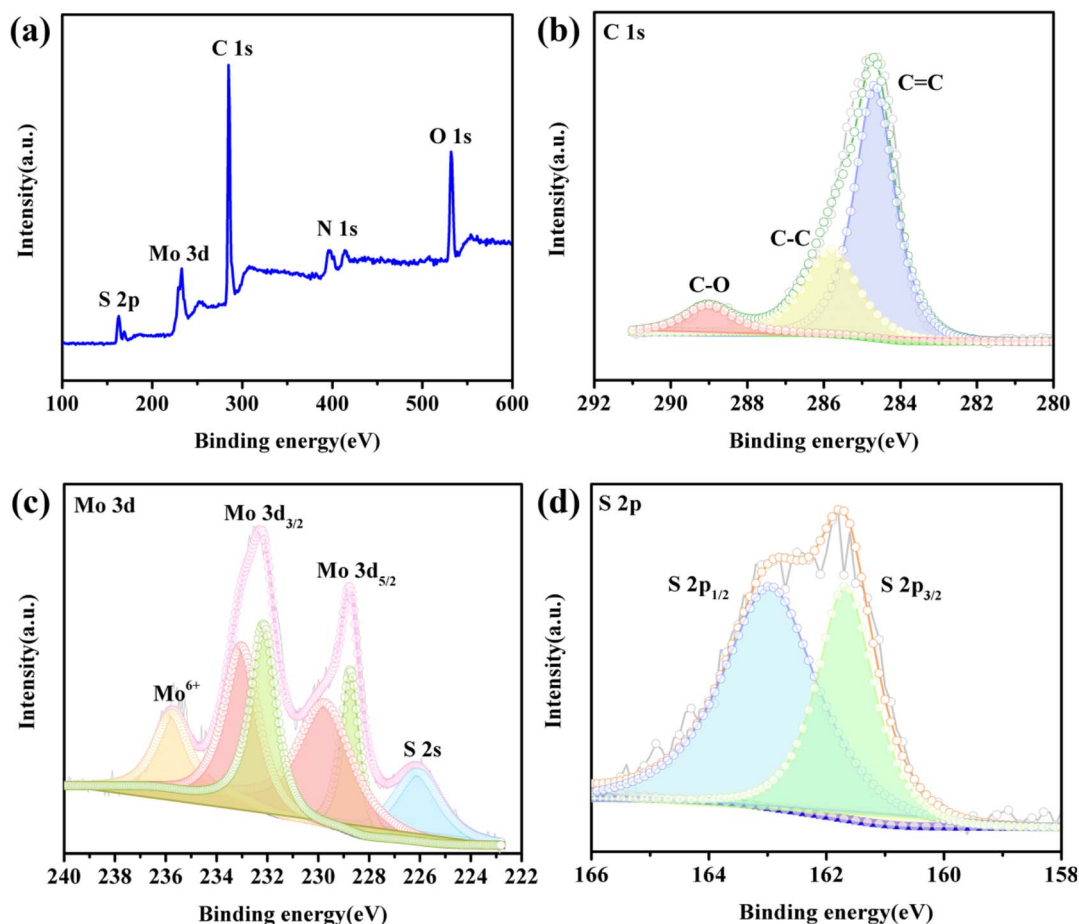


Fig. 3 XPS (a) survey, (b) C 1s, (c) Mo 3d and (d) S 2p spectra of MoS₂-CNT nanozyme.

POD-like activity of MoS₂-CNT nanozyme

Pure CNTs, MoS₂ NSs and MoS₂-CNT nanozyme were used as catalysts to oxidize TMB in the presence of H₂O₂ to determine their activity. The reaction system included 20.0 μL 30.0% H₂O₂ solution, 40.0 μL 1.00 mg mL⁻¹ catalyst, and 40.0 μL 10.0 mmol L⁻¹ TMB. After 40 min at 10 °C, the absorbance of the reaction system was recorded at 652 nm. As shown in Fig. 4a, the CNTs only weakly oxidized TMB in the presence of H₂O₂. Under the

same conditions, the oxidation capacity of the MoS₂ NSs for TMB was significantly stronger than that of the CNTs. When the CNTs and MoS₂ NSs formed the MoS₂-CNT compound, its catalytic ability was better than that when they existed individually. This may be due to the synergistic effect between the CNTs and MoS₂ to improve their catalytic performance. Alternatively, the introduction of CNTs expanded the interlayer distance and specific surface area of the MoS₂ NSs, which is conducive to their contact with the substrate. In contrast, the

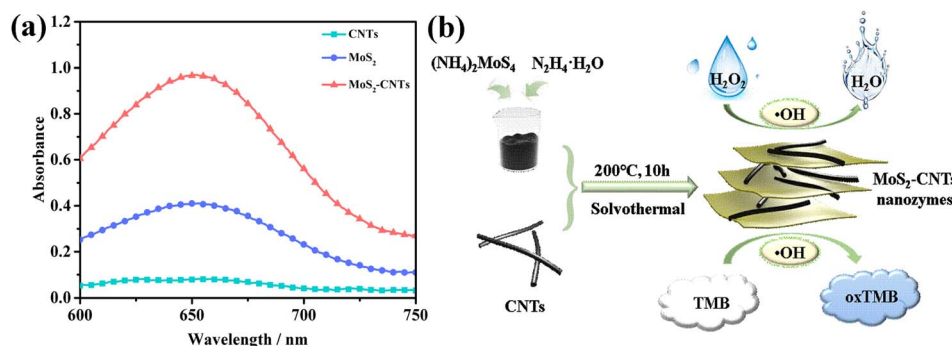


Fig. 4 (a) UV-vis spectra of CNTs, MoS₂ and MoS₂-CNT nanozyme as a catalyst in the TMB-H₂O₂ reaction system, respectively. (b) Catalytic schematic of MoS₂-CNT nanozyme toward the oxidation of TMB in the presence of H₂O₂.



MoS₂-CNT nanozyme had the strongest oxidation effect on TMB in the presence of H₂O₂, and thus this material was used in the following experiments. To prove that the color change is caused by TMB and H₂O₂ catalyzed by the MoS₂-CNT nanozyme, the absorption spectra of different reaction systems under the same conditions were measured, and the results are shown in Fig. S2.† As can be seen, only when MoS₂-CNTs, TMB and H₂O₂ were present simultaneously, an obvious absorption peak appeared at 652 nm. The inset also shows that the color changes in the reaction system occurred only when all three were present together. This indicates that the MoS₂-CNT nanozyme has intrinsic POD-like activity. According to previously reported work, it is known that MoS₂ nanozyme can decompose H₂O₂ under acidic conditions to produce hydroxyl radicals ([•]OH), which can further oxidize the colorless TMB to obtain a blue product. Therefore, it can be inferred that the MoS₂-CNT nanozyme may also have a similar catalytic mechanism. A schematic of the catalytic effect of the MoS₂-CNT nanozyme toward the oxidation of TMB in the presence of H₂O₂ is shown in Fig. 4b.

Optimization of POD-like catalytic conditions

It is well known that the catalytic activity of any catalyst is related to the reaction conditions. Therefore, the influence of reaction time, temperature, pH and substrate concentration on the POD-like performance of the MoS₂-CNT nanozyme was measured by varying the time (5–45 min), temperature (5–45.0 °C), pH (3.00–7.00) and TMB concentration (0.100–1.00 mmol L^{−1}), respectively. Only one of these conditions was changed in each experiment, and the maximum absorbance value for every condition was set to 100%. The ratio of the other value to the maximum value was named the relative activity. As shown in Fig. S3a,† with time, the absorbance of the reaction system increased initially, and then decreased, reaching the highest at 40 min. Thus, 40 min was chosen as the best reaction time. Fig. S3b† shows that when the reaction temperature changed between 5.00 °C and 45.0 °C, with an increase in temperature, the absorbance value increased initially, and then decreased, finally tending to be stable. Thus, the optimum reaction temperature was 10.0 °C. This showed that the catalytic activity of the nanozyme was higher at low temperature. This may be due to the fact that the increase in temperature can easily lead to the decomposition of H₂O₂, which causes the intermediate to be tightly adsorbed on the surface of the catalyst and hinders the exposure of the active sites of the enzyme, thus inhibiting its catalytic activity. When the temperature was 15.0 °C, the absorbance value was still maintained by more than 85.0%. Therefore, the optimum reaction temperature for the nanozyme can be selected according to the actual situation in the range of 5.00–15.0 °C. The analysis of the effect of pH on the activity of the MoS₂-CNT nanozyme is shown in Fig. S3c.† The results reveal that the catalyzed reaction can only take place under acidic conditions. Also, with an increase in pH, the absorbance showed a trend of increasing initially, and then decreased, where the catalytic activity was the highest at pH 4.00. Therefore, buffer solution with pH 4.00 was the best choice for the

reaction. The effect of substrate concentration on the POD-like activity of the MoS₂-CNT nanozyme is shown in Fig. S3d.† When the concentration of TMB varied in the range of 0.100–0.800 mmol L^{−1}, the POD-like activity of MoS₂-CNT increased with an increase in the substrate concentration. However, when the concentration of TMB varied in the range of 0.100–0.800 mmol L^{−1}, the POD-like activity of MoS₂-CNTs decreased. Thus, the concentration of 0.800 mmol L^{−1} substrate TMB was the best choice to maximize the performance of MoS₂-CNTs. In summary, the catalytic property of the MoS₂-CNT nanozyme is similar to that of natural enzymes, which is dependent on temperature, pH, substrate concentration and reaction time. The optimal conditions were selected in this work as follows: temperature of 10.0 °C, pH of 4.00, concentration of TMB of 0.800 mmol L^{−1} and reaction time of 40.0 min.

Steady-state of the MoS₂-CNT nanozyme

The catalytic properties of the MoS₂-CNT nanozyme were systematically studied by first-order reaction kinetics. Fig. 5a and c show Michaelis–Menten curves of TMB and H₂O₂, respectively. As shown in Fig. 5b and d, when the concentration of H₂O₂ was fixed and the concentration of TMB changed between 0.1–0.7 mmol L^{−1}, the reciprocal of concentration was linearly related to the reciprocal of the reaction rate, and the linear equation is $y = 1 \times 10^7 x + 1 \times 10^7$ ($R^2 = 0.9915$). On the contrary, when the concentration of TMB was fixed and the concentration of H₂O₂ changed between 1–50 mmol L^{−1}, the reciprocal of concentration was linearly related to the reciprocal of the reaction rate, and the linear equation is $y = 4 \times 10^8 x + 3 \times 10^7$ ($R^2 = 0.9953$). The kinetic constants K_m and V_{max} were calculated using the Lineweaver–Burk plots and listed in Table 1.

K_m represents the affinity of the catalyst to the substrate, where a lower value of K_m indicates higher affinity between the two.³² The K_m value of MoS₂-CNT nanozyme towards H₂O₂ was 13-fold higher than that towards TMB. This indicated that the MoS₂-CNT nanozyme had apparently higher affinity for TMB than H₂O₂. Compared with natural HRP and Co₃O₄ nanozyme, the MoS₂-CNT nanozyme had a lower K_m value for TMB, which proved that it has stronger catalytic activity.³³ In addition, the V_{max} value for H₂O₂ for the MoS₂-CNT nanozyme was higher than that of HRP, indicating that less MoS₂-CNT nanozyme was needed to achieve the same reaction rate.

Colorimetric determination of H₂O₂

Based on the optimum assay conditions, a colorimetric method for the determination of H₂O₂ was established by using the MoS₂-CNT nanozyme. The absorbance at the wavelength of 652 nm varied with the concentration of H₂O₂, as shown in Fig. 6a. The plot shows good linearity ($R^2 = 0.994$) between the absorbance value and concentration of H₂O₂ from 5.00 to 500 μmol L^{−1}. The linear equation is $y = 3.00 \times 10^{-4} x + 0.0878$, where “y” is the absorbance value and “x” is the concentration of H₂O₂. Further, the corresponding LOD was calculated to be 1.40 μmol L^{−1} according to the signal-to-noise ratio (S/N = 3). Compared with the previously reported literature, the constructed MoS₂-CNT/TMB–H₂O₂ sensing platform has a wide



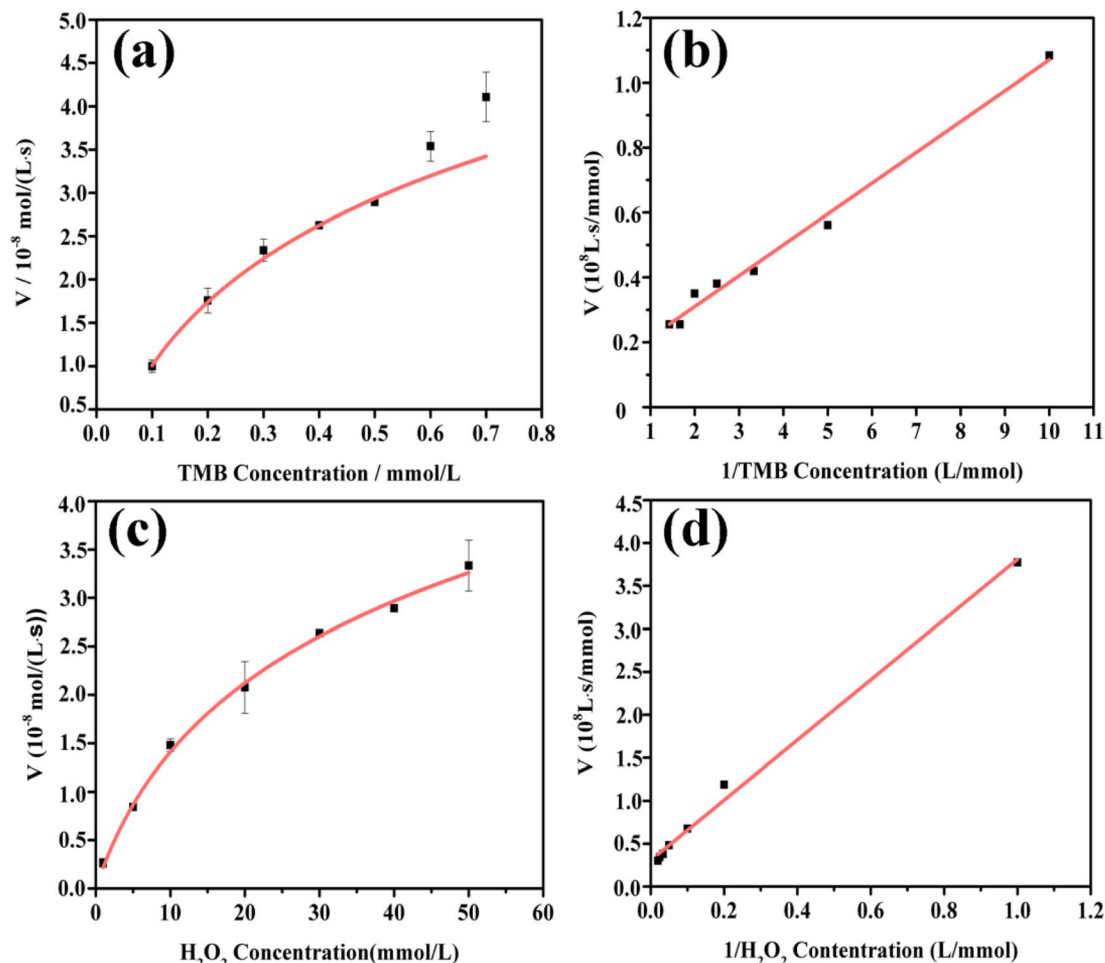


Fig. 5 Steady-state kinetic assay of MoS₂-CNT nanozyme: (a) and (c) Michaelis–Menten curves of TMB and H₂O₂ with different concentrations and (b) and (d) are Lineweaver–Burk plots of TMB and H₂O₂, respectively.

Table 1 Comparison of the kinetic parameters between MoS₂-CNT nanozyme and other enzymes

No.	Enzyme	Substrate	K_m (mmol L ⁻¹)	V_{max} (10 ⁻⁸ mol L ⁻¹ s)	Ref.
1	HRP	TMB	3.95	37.7	34
		H ₂ O ₂	10.4	0.689	
2	Co ₃ O ₄	TMB	5.09	9.98	35
		H ₂ O ₂	1.14	1.72	
3	MoS ₂ -CNT	TMB	1.00	10.0	This work
		H ₂ O ₂	13.2	3.33	

linear range and low LOD (listed in Table 2). Thus, it showed a good H₂O₂ determination performance.

Selectivity and stability

Anti-interference is one of the important parameter for sensors.³⁶ Thus, to test the sensitivity of the MoS₂-CNT/TMB/H₂O₂ colorimetric detection platform, control experiments were carried out. Considering that soda water may contain carbohydrates, ions, vitamins, amino acids and other substances, glucose, sucrose, citric acid, AA,

Na⁺, K⁺, NH₄⁺, Ca²⁺, Cl⁻, CO₃²⁻, Arg, Lys and Cys with 10-fold H₂O₂ concentration were respectively used as interferents, and

the absorbance value at a wavelength of 652 nm was determined using the same reaction conditions as above. As shown in Fig. 6b, the reaction system with these interferents as a substrate had a low absorbance value, and only when H₂O₂ was used as the substrate, the absorbance increased significantly. This indicates that the proposed colorimetric detection platform has satisfactory sensitivity.

Stability is another significant indicator for sensors. To evaluate the long-term stability of the developed colorimetric detection platform, it was stored in the natural environment and was measured continuously for three weeks. As shown in Fig. 6c, when it was stored for up to 3 weeks, it still maintained



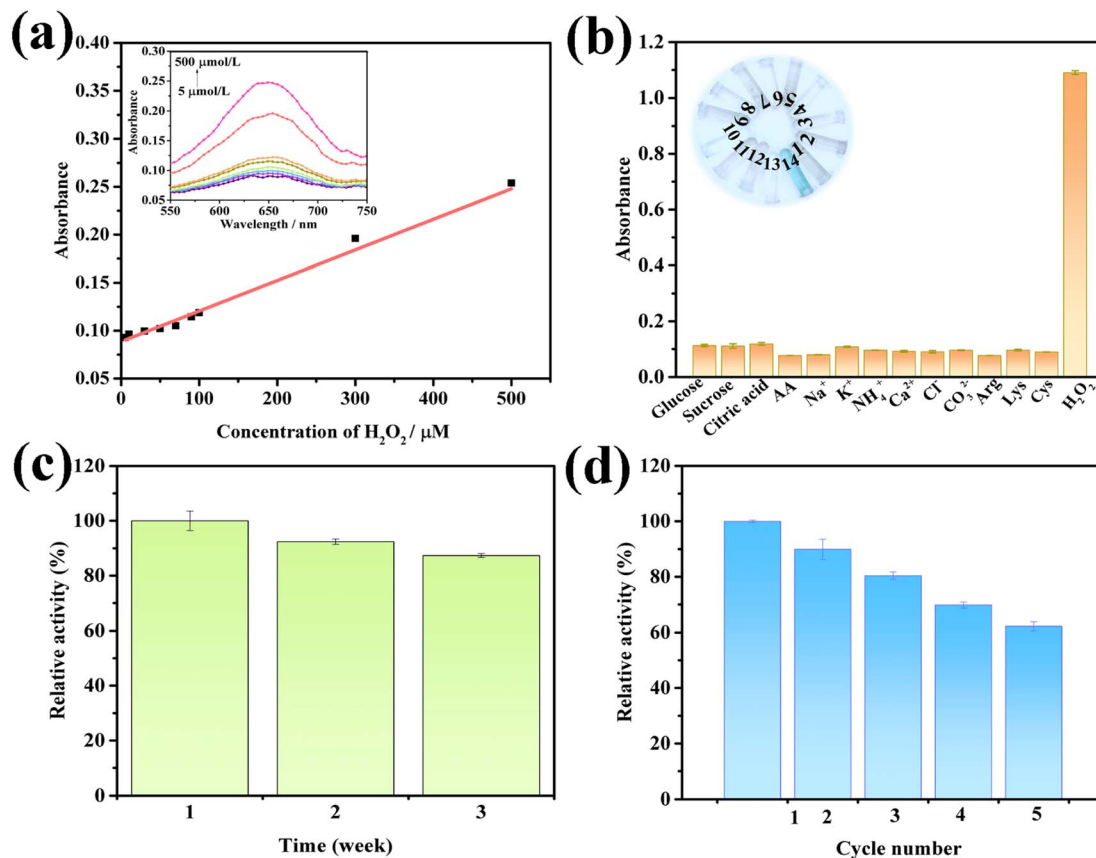


Fig. 6 (a) Calibration curve of H₂O₂ concentration vs. absorbance at 652 nm (inset: corresponding absorption spectrum curve). (b) Selectivity analysis of MoS₂-CNT/TMB system for the determination of H₂O₂ (concentration of H₂O₂: 100 μmol L⁻¹ and concentration of each interfering substrate: 1 mmol L⁻¹) (inset: colors of determination method with various saccharides, No. 1–14 correspond to the abscissa from left to right, respectively). (c) Long-term stability analysis of the as-prepared MoS₂-CNT nanozyme. (d) Reproducibility results of the colorimetric method.

Table 2 Comparison of different nanozymes for the colorimetric determination H₂O₂

Nanozyme	Method	Liner range (μmol L ⁻¹)	LOD (μmol L ⁻¹)	Ref.
GO-FeTPyP NCs	Colorimetric	20.0–500	72.0	37
FePt–Au HNPs	Colorimetric	20.0–700	12.0	38
Co ₃ O ₄ ·NPs	Colorimetric	50.0–2.50 × 10 ⁴	10.0	39
Fe ₃ O ₄ @Cu@Cu ₂ O	Colorimetric	4.00 × 10 ³ –5.00 × 10 ⁴	2.00 × 10 ³	40
MoS ₂ -CNTs	Colorimetric	5.00–500	1.40	This work

its peroxidase-like activity by more than 87.0%, indicating that the developed detection platform has good stability. The reproducibility results of the colorimetric determination method established in this work are displayed in Fig. 6d. The relative activity was maintained as high as 80.4% after reuse for 3 times, while it was 62.3% after 5 times. Consequently, the prepared MoS₂-CNT nanozyme can be reused for the colorimetric determination of H₂O₂ at least 3 times.

Application in actual samples

H₂O₂ is widely applied in the agriculture and food fields. In beverage production, for example, it is often used as an anti-putrefactive and stabilizer. However, excessive residual H₂O₂

may lead to serious consequences for human health. Therefore, it is of great significance to detect residual H₂O₂ in food and beverages.⁴¹ To evaluate the analytical performance of the colorimetric determination platform, the contents of H₂O₂ in

Table 3 Recovery tests in soda water samples using the MoS₂-CNT/TMB/H₂O₂ platform (n = 3)

Added (μmol L ⁻¹)	Found (μmol L ⁻¹)	Recovery (%)	RSD (%)
50.0	53.7	107	1.6
100	94.9	94.9	0.6
300	277	92.3	0.5



soda water were measured using the spiked recovery method. As shown in Table 3, the relative standard deviation (RSD) of the three parallel samples was less than 2.00%, and the recovery rate was between 92.3–107%. In summary, the proposed approach can be used as a promising sensing platform for the determination of H₂O₂ with the merits of specificity, sensitivity and reliability.

Conclusion

In conclusion, using one-step solvothermal reduction, the 2D–1D MoS₂–CNT nanozyme was synthesized. Under acidic conditions, it could turn the colorless TMB oxide blue oTMB in the presence of H₂O₂, showing excellent POD-like activity. The kinetic studies showed that the MoS₂–CNT nanozyme had better catalytic performance than natural HRP. After the experimental conditions were optimized, a sensitive MoS₂–CNT/TMB/H₂O₂ colorimetric platform was constructed with a linear range from 5.00 to 500 μmol L^{−1} and LOD of 1.40 μmol L^{−1}. The developed detection platform exhibited favorable selectivity, stability and reproducibility. Further, the colorimetric method was applied for the determination of H₂O₂ in soda water with good reliability.

Conflicts of interest

There are no conflicts to declare.

Acknowledgements

This work was supported by the Joint Funds of Inner Mongolia autonomous region (2021LHMS02002).

References

- 1 D. Zhang, N. Shen, J. Zhang, J. Zhu, Y. Guo and L. Xu, *RSC Adv.*, 2020, **10**, 8685–8691.
- 2 J. Wu, X. Wang, Q. Wang, Z. Lou, S. Li, Y. Zhu, L. Qin and H. Wei, *Chem. Soc. Rev.*, 2019, **48**, 1004–1076.
- 3 H. Wei and E. Wang, *Chem. Soc. Rev.*, 2013, **42**, 6060–6093.
- 4 X. Wang, Y. Hu and H. Wei, *Inorg. Chem. Front.*, 2016, **3**, 41–60.
- 5 X. Wang, L. Qin, M. Zhou, Z. Lou and H. Wei, *Anal. Chem.*, 2018, **90**, 11696–11702.
- 6 T. T. L. Souza, M. L. Moraes and M. Ferreira, *Sens. Actuators, B*, 2013, **178**, 101–106.
- 7 C. P. Lu, C. T. Lin, C. M. Chang, S. H. Wu and L. C. Lo, *J. Agric. Food Chem.*, 2011, **59**, 11403–11406.
- 8 X. Wu, Y. Zhang, T. Han, H. Wu, S. Guo and J. Zhang, *RSC Adv.*, 2014, **4**, 3299–3305.
- 9 P. Makvandi, C. Y. Wang, E. N. Zare, A. Borzacchiello, L. N. Niu and F. R. Tay, *Adv. Funct. Mater.*, 2020, **30**, 1910021.
- 10 Z. Liu, B. Zhao, Y. Shi, C. Guo, H. Yang and Z. Li, *Talanta*, 2010, **81**, 1650–1654.
- 11 C. Guo, Y. Song, H. Wei, P. Li, L. Wang, L. Sun, Y. Sun and Z. Li, *Anal. Bioanal. Chem.*, 2007, **389**, 527–532.
- 12 W. Dong, G. Chen, X. Hu, X. Zhang, W. Shi and Z. Fu, *Sens. Actuators, B*, 2020, 305.
- 13 X. Zhang, C. Wang and Y. Gao, *Microchim. Acta*, 2020, 187.
- 14 X. Zhang and Y. Gao, *Chem. – Asian J.*, 2020, **15**, 1315–1323.
- 15 K. Zhou, J. Liu, Y. Shi, S. Jiang, D. Wang, Y. Hu and Z. Gui, *ACS Appl. Mater. Interfaces*, 2015, **7**, 6070–6081.
- 16 C. Zhao, C. Yu, M. Zhang, Q. Sun, S. Li, M. N. Banis, X. Han, Q. Dong, J. Yang, G. Wang, X. Sun and J. Qiu, *Nano Energy*, 2017, **41**, 66–74.
- 17 X. Zhang, A. Selkirk, S. Zhang, J. Huang, Y. Li, Y. Xie, N. Dong, Y. Cui, L. Zhang, W. J. Blau and J. Wang, *Chem. – Eur. J.*, 2017, **23**, 3321–3327.
- 18 W. Guo, X. Li, L. Cui, Y. Li, H. Zhang and T. Ni, *Bioprocess Biosyst. Eng.*, 2022, **45**, 159–170.
- 19 W. Liu, S. He, Y. Wang, Y. Dou, D. Pan, Y. Feng, G. Qian, J. Xu and S. Miao, *Electrochim. Acta*, 2014, **144**, 119–126.
- 20 W. Han, Y. Xia, D. Yang and A. Dong, *Chem. Commun.*, 2021, **57**, 4400–4403.
- 21 Y. Xu, P. E. Pehrsson, L. Chen and W. Zhao, *J. Am. Chem. Soc.*, 2008, **130**, 10054.
- 22 M. Chen, Y. Dai, J. Wang, Q. Wang, Y. Wang, X. Cheng and X. Yan, *J. Alloys Compd.*, 2017, **696**, 900–906.
- 23 Y. Song, X. Wang, C. Zhao, K. Qu, J. Ren and X. Qu, *Chem. – Eur. J.*, 2010, **16**, 3617–3621.
- 24 W. Gu, Y. Yan, C. Zhang, C. Ding and Y. Xian, *ACS Appl. Mater. Interfaces*, 2016, **8**, 11272–11279.
- 25 J. Y. Lin, A. L. Su, C. Y. Chang, K. C. Hung and T. W. Lin, *Chemelectrochem*, 2015, **2**, 720–725.
- 26 H. Zhou, R. Zhang, S. Song, C. Xiao, G. Gao and S. Ding, *ACS Appl. Energy Mater.*, 2018, **1**, 5112–5118.
- 27 W. W. Xu, X. L. Dong, Y. Wang, N. Zheng, B. R. Zheng, Q. Lin and Y. L. Zhao, *Chemistryselect*, 2020, **5**, 13603–13608.
- 28 I. Zafiropoulou, M. S. Katsiotis, N. Boukos, M. A. Karakassides, S. Stephen, V. Tzitzios, M. Fardis, R. V. Vladea, S. M. Alhassan and G. Papavassiliou, *J. Phys. Chem. C*, 2013, **117**, 10135–10142.
- 29 C. M. Chen, M. Chen, F. C. Leu, S. Y. Hsu, S. C. Wang, S. C. Shi and C. F. Chen, *Diamond Relat. Mater.*, 2004, **13**, 1182–1186.
- 30 S. Anwer, Y. Huang, B. Li, B. Govindan, K. Liao, W. J. Cantwell, F. Wu, R. Chen and L. Zheng, *ACS Appl. Mater. Interfaces*, 2019, **11**, 22323–22331.
- 31 H. Chen, T. Song, L. Tang, X. Pu, Z. Li, Q. Xu, H. Liu, Y. Wang and Y. Xia, *J. Power Sources*, 2020, 445.
- 32 M. Hosseini, F. S. Sabet, H. Khabbaz, M. Aghazadeh, F. Mizani and M. R. Ganjali, *Anal. Methods*, 2017, **9**, 3519–3524.
- 33 H. Liu, M. Jiao, C. Gu and M. Zhang, *J. Alloys Compd.*, 2018, **741**, 197–204.
- 34 K. Fan, H. Wang, J. Xi, Q. Liu, X. Meng, D. Duan, L. Gao and X. Yan, *Chem. Commun.*, 2017, **53**, 424–427.
- 35 J. Luo, J. Wang, G. Li, Q. Huo and Y. Liu, *Chem. Commun.*, 2013, **49**, 11433–11435.
- 36 J. Chen, Y. Shu, H. Li, Q. Xu and X. Hu, *Talanta*, 2018, **189**, 254–261.



- 37 C. Socaci, F. Pogacean, A. R. Bins, M. Coros, M. C. Rosu, L. Magerusan, G. Katona and S. Pruneanu, *Talanta*, 2016, **148**, 511–517.
- 38 Y. Ding, B. Yang, H. Liu, Z. Liu, X. Zhang, X. Zheng and Q. Liu, *Sens. Actuators, B*, 2018, **259**, 775–783.
- 39 J. Mu, Y. Wang, M. Zhao and L. Zhang, *Chem. Commun.*, 2012, **48**, 2540–2542.
- 40 Z. Wang, M. Chen, J. Shu and Y. Li, *J. Alloys Compd.*, 2016, **682**, 432–440.
- 41 Z. Hu, Y. Yin, Q. Liu and X. Zheng, *Analyst*, 2019, **144**, 2716–2724.

